Enhancement of Graphene Phonon Excitation by a Chemically Engineered Molecular Resonance

Xiaocui Wu,[1] Nicolas Néel,[1] Mads Brandbyge,[2] and Jörg Kröger[1,*]
[1]Institut für Physik, Technische Universität Ilmenau, D-98693 Ilmenau, Germany
[2]Center of Nanostructured Graphene, Department of Physics, Technical University of Denmark, DK-2800 Kongens Lyngby, Denmark

(Received 18 October 2022; accepted 21 February 2023; published 13 March 2023)

The abstraction of pyrrolic hydrogen from a single phthalocyanine on graphene turns the molecule into a sensitive probe for graphene phonons. The inelastic electron transport measured with a scanning tunneling microscope across the molecular adsorbate and graphene becomes strongly enhanced for a graphene out-of-plane acoustic phonon mode. Supporting density functional and transport calculations elucidate the underlying physical mechanism. A molecular orbital resonance close to the Fermi energy controls the inelastic current while specific phonon modes of graphene are magnified due to their coupling to symmetry-equivalent vibrational quanta of the molecule.

DOI: 10.1103/PhysRevLett.130.116201

Inelastic electron tunneling spectroscopy (IETS) is most relevant to unraveling mechanisms underlying the excitation of vibrational quanta [1,2] and photon emission [3–7] as well as single-atom spin-flip transitions [8]. After the initial report on IETS of molecular vibrations in planar tunneling junctions [1], a seminal work demonstrated the acquisition of single-molecule vibrational spectra with a scanning tunneling microscope (STM) [2]. The amount of ensuing reports on IETS of molecular vibrations is substantial and has been reviewed in other articles [9–14]. Very often, the change in the differential conductance (dI/dV: I, current; V, voltage) due to vibrational quantum excitation is on the order of only a few percent or is even compensated by virtual excitations in the elastic electron transport channel [15–18]. Exceptions can occur in the case of resonant enhancement [19–24], where a molecular orbital resonance close to the Fermi energy (E_F) overlaps with energies of molecular vibrational quanta and increases the residence time of the injected charge carrier for efficient energy transfer to the vibrational degrees of freedom of the molecule.

In contrast to molecular vibrations, reports on lattice phonons using STM-IETS are scarce. Phonon signals from graphite [25], $Bi_2Sr_2CaCu_2O_{8+\delta}$ [26], Au(111) [27,28], Cu(111) [27], Ag(100) [29], and Cu(110) [30] were measured across STM junctions. Extraordinarily strong phonon signals were observed for quasi-free graphene on SiO_2 [31,32], which stimulated the advent of phonon-mediated tunneling [31]. The inelastic tunneling electrons can reach Dirac cone final states at the K-point of the Brillouin zone (BZ) by the emission of a graphene phonon with an appropriate wave vector. The mechanism was later extended by inclusion of the phonon density of states (DOS) [33,34], the electron–phonon coupling, and the electrode–graphene hybridization [35,36] in order to be applicable to graphene on metal surfaces as well [34–38]. While the local probing of graphene phonons with STM-IETS is rare, laterally averaging spectroscopies have very frequently been used, as thoroughly described in a previous report [39].

The work presented here reveals two novelties. First, the orbital resonance of an adsorbate—a phthalocyanine molecule—enhances the phonon IETS signal of the substrate—graphene. Second, the quasi-free state of graphene and, thus, phonon-mediated tunneling are not required for the phonon signal enhancement. These new insights have been inferred from IETS experiments performed on $C_{32}H_{18}N_8$ (2H-Pc) as well as on its pyrrolic-H-abstracted variant Pc adsorbed on graphene-covered Ir(111). While intact 2H-Pc does not give rise to any vibrational signature in the spectra, in agreement with the absence of phonon signals of graphene on Ir(111) [34], charge injection into Pc leads to strong inelastic excitations whose energies are compatible with molecular vibrations and graphene phonons. The physical mechanisms underlying these observations are unveiled by the accompanying density functional theory (DFT) and transport calculations. The removal of pyrrolic H induces an orbital resonance close to E_F, which is absent for the intact molecule. Importantly, while the molecular orbital resonance enhances the inelastic electron transport across the junction, the magnification of specific graphene phonon signals is driven by the coupling of symmetrically equivalent molecule and graphene vibrations.

Figure 1(a) illustrates, with ball-and-stick models of the molecules, the abstraction of pyrrolic H. The top model (2H-Pc) exhibits two central H atoms, each covalently bonded to an N atom of the opposite pyrrole moieties. Such intact molecules appear with a crosslike shape and nearly uniform contrast in STM images [40], with the exception of a central depression [Fig. 1(b)]. The STM topograph further

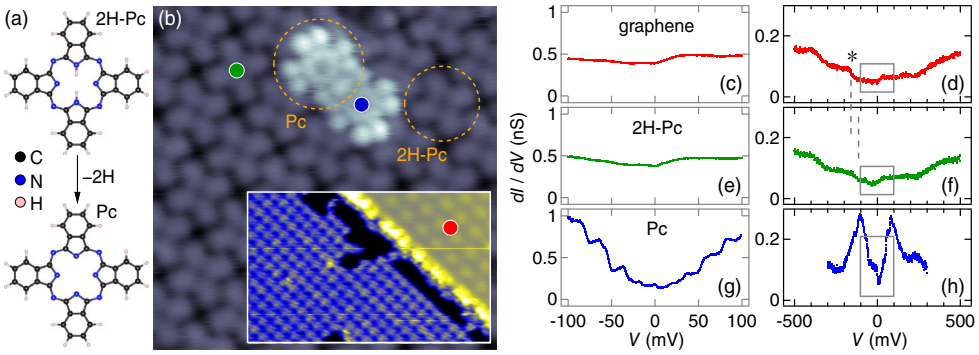

FIG. 1. (a) Ball-and-stick models of 2H-Pc and Pc. (b) STM image of molecule-covered graphene on Ir(111) (sample voltage: 0.78 V; tunneling current: 25 pA; size: 8 nm × 8 nm). The 2H-Pc and Pc molecules are marked by dashed circles. Inset: overview STM image with 2H-Pc-covered graphene (left) adjacent to pristine graphene (right) with the characteristic hexagonal Moiré pattern (0.81 V, 30 pA, 30 nm × 19 nm). (c)–(h) Spectra of dI/dV acquired atop positions marked by dots in (b), i.e., atop (c),(d) graphene, and the center of (e),(f) 2H-Pc and (g),(h) Pc. Rectangles in panels (d), (f), and (h) mark the region of spectroscopic data in panels (c), (e), and (g). The asterisk in panel (d) indicates the signature of an Ir(111) surface resonance that exhibits a shift upon 2H-Pc adsorption [dashed lines in panels (d) and (f)]. Feedback loop parameters: (c),(e),(g) 0.1 V; (d),(f) 0.5 V; (h) 0.3 V and 50 pA.

reveals that room-temperature deposition of 2H-Pc on graphene-covered Ir(111) leads to a molecular superstructure with a square primitive unit cell [41,58,59]. The pyrrolic H can be removed from the macrocycle by placing the STM tip atop the center of 2H-Pc, deactivating the feedback loop at 1 V, 10 pA and ramping the bias voltage up to 3.3 V [41]. The resulting product Pc molecule appears with brighter contrast and submolecular structural motifs in STM images [Fig. 1(b)]. It was previously shown that the intramolecular contrast of Pc is due to the spatial distribution of the highest occupied molecular orbital (HOMO) that depopulates in the course of pyrrolic-H detachment [41].

The key experimental finding reported here is the marked difference of dI/dV spectra acquired atop pristine graphene [Figs. 1(c) and 1(d)], intact 2H-Pc [Figs. 1(e) and 1(f)], and pyrrolic-H-abstracted Pc [Figs. 1(g) and 1(h)] on graphene. In the explored voltage ranges, $|V| \leq 100$ mV [Figs. 1(c), 1(e), and 1(g)] and $|V| \leq 500$ mV [Figs. 1(d), 1(f), and 1(h)], spectra of graphene and 2H-Pc are virtually identical. The absence of the K-point Dirac cone from dI/dV data is due to its rapidly decaying wave function [60]. A Γ-point Ir(111) surface resonance close to E_F ($V = 0$ in the spectra) contributes strongly to the tunneling current [asterisk in Fig. 1(d)] and masks the Dirac cone signature [60]. Upon 2H-Pc, this resonance shifts by approximately 40 meV toward E_F. Intriguingly, the situation changes strongly for dI/dV spectra recorded atop the center of Pc. Pronounced steplike signatures occur that are symmetrically positioned at positive and negative voltages [Fig. 1(g), steps at ±15 mV, ±32 mV, ±53 mV, ±60 mV, ±78 mV]. Moreover, the steps are generally more pronounced for negative voltage, exceeding, for instance, a factor 2 for the signature at ±32 mV. An enlarged view of these data, together with a d^2I/dV^2 spectrum, is presented in the Supplemental Material [40]. Figure 1(h) additionally reveals that the dI/dV steps are superimposed with broad resonances peaked at −100 mV and 82 mV. Such resonances are absent from the spectra observed for graphene and intact 2H-Pc. A minority of Pc molecules give rise to a resonance energy shifted well above E_F and, concomitantly, to strongly attenuated inelastic signals [40]. Most likely, these molecules reside at graphene lattice defects that caused a different charge transfer compared to the majority of Pc decorating intact graphene. This hints at the role of the molecular resonance and its position within the range of vibrational energies around E_F for understanding the observed effect, as discussed below.

It is tempting to associate molecular vibrational quanta with the dI/dV steps. An ambiguity in this assignment arises, however, due to graphene phonons with similar energies, in particular, due to an out-of-plane acoustic phonon at the M point (49 meV) of the BZ as well as degenerate transverse acoustic and out-of-plane optical phonons at M (80 meV) [34,35,61]. The computational results to be discussed below will resolve this ambiguity. Prior to presenting the underlying theory, additional experimental data characterize the spatial variation of dI/dV spectra.

Figure 2 shows spatially resolved dI/dV spectra acquired atop the pyrrole [Figs. 2(a) and 2(b)] and the benzene [Figs. 2(c) and 2(d)] moiety of Pc. Compared to the spectra atop the Pc center [Fig. 1(g)], the steplike changes in dI/dV are attenuated above the pyrrole group and entirely suppressed atop benzene. The resonance pair around zero bias is still present with different peak voltages, i.e., at −122 mV, 127 mV atop pyrrole and at −180 mV, 56 mV atop benzene. These resonances may be due to p_z states of the molecule with ample spectral weight at the benzene moieties [41].

To interpret the data, inelastic transport calculations based on DFT and nonequilibrium Green function methods [42] at the generalized-gradient approximation [43] level

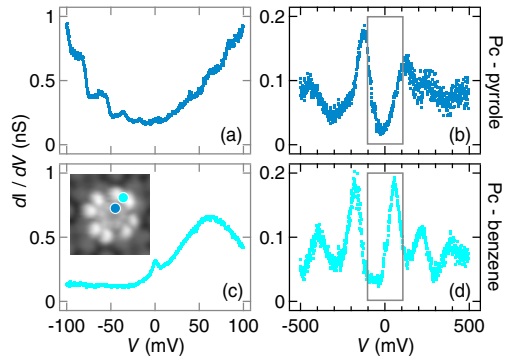

FIG. 2. Spectra of dI/dV acquired atop (a),(b) a pyrrole and (c), (d) a benzene moiety of Pc on graphene-covered Ir(111). Inset to (c): STM image (1 V, 10 pA, 2.5 nm × 2.5 nm) of Pc embedded in a 2H-Pc island with marked (dots) positions of spectroscopy. Rectangles in panels (b) and (d) mark the region of spectroscopic data in panels (a) and (c). Feedback loop parameters are as follows: (a),(c) 0.1 V; (b),(d) 0.5 V and 50 pA.

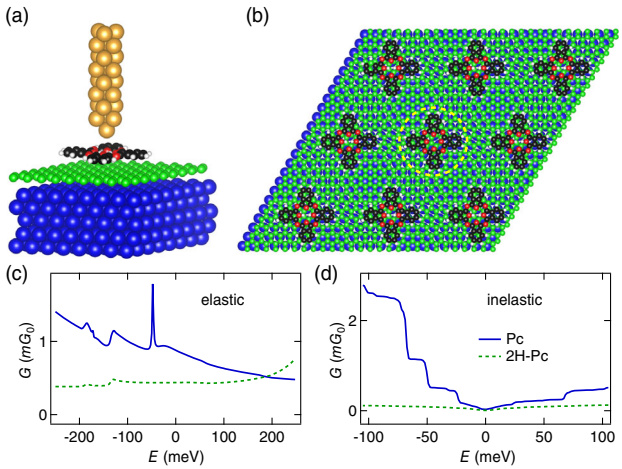

FIG. 3. (a) Side and (b) top views of the unit cell used in the simulations. (c) Elastic electron transmission function for Pc (solid line) and 2H-Pc (dashed line) as a function of energy ($E_F = 0$). (d) Inelastic electron transmission for Pc and 2H-Pc. G_0 denotes the quantum of conductance.

were used. The model setup is presented in Figs. 3(a) and 3(b) where 2H-Pc (or Pc) is positioned atop graphene on a static Ir(111) substrate [40]. The molecule–graphene and graphene–surface distances are set to 0.32 nm as previously determined [41]. The simulations use a Au tip that matches the Au-coated W tip apex in the experiment [40] and the Tersoff-Hamann approximation of a spherical tip wave function [62,63]. The tip is placed symmetrically above the molecule with a vertical distance of 0.4 nm to the molecular center. Individually relaxed geometries are used for the model elements; i.e., the impact of the interactions is neglected. Self-energies describe open-electrode regions, which are in the Ir and Au electrodes as well as in the infinite graphene with adsorbed 2H-Pc (or Pc). For the calculations of elastic and inelastic electron transmissions, the molecular supercell of the experiment is used [Fig. 3(b)]; that is, a Pc molecule (dashed circle) is surrounded by intact 2H-Pc molecules.

The resulting elastic conductance of the junction is plotted in Fig. 3(c) for Pc (solid line) and 2H-Pc (dashed line). The most obvious change is the overall increase of the elastic transmission, which may be due to the increased symmetry of Pc and its electronic states that facilitate the electron transport between a spherically symmetric tip and graphene via the molecule [64]. The resonant transmission behavior close to E_F in the case of Pc will be most important for the discussion of the inelastic electron transport. Calculations of the projected DOS [40] unveil that the transmission resonances closest to E_F can be associated with the Pc molecule alone. They are due to the degenerate HOMO [41] with a more weakly (sharp resonant feature) and more strongly (broad signature) coupled linear combination of the HOMO states to the substrate.

The inelastic differential conductance [Fig. 3(d)] is computed in the lowest-order perturbation of the electron–vibration coupling [44,45] using the expression

$$\frac{dI_i}{dV} = \sum_{\lambda,\sigma} \gamma_{\lambda,\sigma} \frac{\partial \mathcal{I}}{\partial V}\left(V - \sigma\frac{\hbar\omega_\lambda}{e}\right) \quad (1)$$

[$\hbar = h/(2\pi)$; h is the Planck constant, and e the elementary charge], where $\gamma_{\lambda,\sigma}$ is the calculated inelastic scattering rate for mode λ with energy $\hbar\omega_\lambda$ and $\partial\mathcal{I}/\partial V(V - \sigma\hbar\omega_\lambda/e)$ represents a broadened step function with a step at bias voltage $\sigma\hbar\omega_\lambda/e$ ($\sigma = \pm 1$). In these calculations, the motion of atoms is excited in the molecule and graphene, while the electron–vibration coupling is restricted to the tip–molecule–graphene region. Pronounced steplike signatures appear in the inelastic conductance trace of Pc (solid line), while they are featureless for 2H-Pc (dashed line) in the explored energy range. This behavior can be understood by the strongly resonant transmission structure of Pc [Fig. 3(c)], which enhances the inelastic electron transport [45]. Besides the energies of inelastic signals at ±23 meV, ±32 meV, ±50 meV, ±68 meV, and ±72 meV, which are in good agreement with the experimentally observed voltages of the abrupt dI/dV changes, the polarity asymmetry is well reproduced, too. Because the Pc orbital resonance comprises occupied states, the latter become active in inelastic electron transport for negative sample bias. It is noteworthy that in simulations that neglect the hybridization with the Ir(111) surface, the results are essentially the same; i.e., strong inelastic transmission is present for Pc and absent for 2H-Pc. This observation strengthens the importance of the Pc orbital resonance.

An important remaining task is the disentanglement of individual vibrational contributions to the total inelastic electron transport. To this end, the inelastic conductance is decomposed into components using the vibrational modes and their weights projected onto the molecule and graphene. From the vibrational mode vector $\mathbf{v}_\lambda$, projections

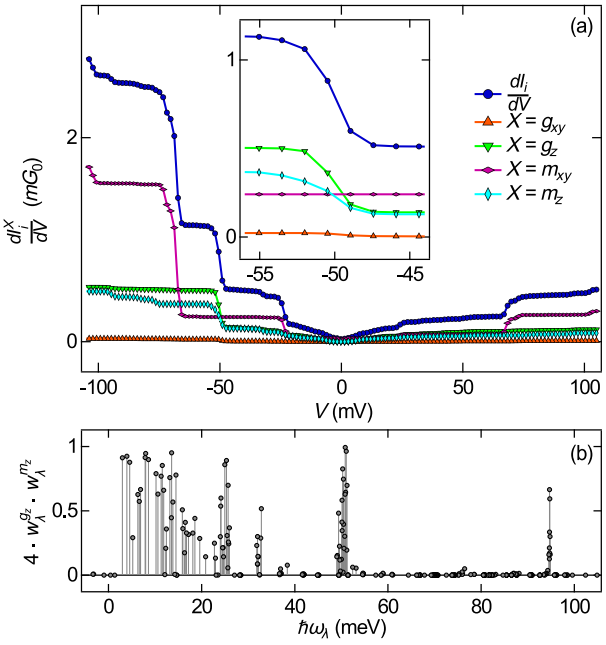

FIG. 4. (a) Phonon inelastic transmission [dI_i^X/dV, Eq. (2)] for Pc decomposed according to phonon mode weights on atoms. Inset: close-up view of an energy range where a graphene out-of-plane phonon (reversed triangles) is particularly strong. (b) Mixing of graphene phonon and Pc vibrational modes with out-of-plane polarization.

onto in-plane (xy) and out-of-plane (z) atom motions of the molecule (m) and graphene (g) are defined and referred to as w_λ^X, with $X \in \{m_{xy}, m_z, g_{xy}, g_z\}$ and $\sum_X w_\lambda^X = 1$ [40]. Individual contributions to dI_i/dV [Eq. (1)] are then defined as

$$\frac{dI_i^X}{dV} = \sum_{\lambda,\sigma} w_\lambda^X \gamma_{\lambda,\sigma} \frac{\partial \mathcal{I}}{\partial V}\left(V - \sigma\frac{\hbar\omega_\lambda}{e}\right). \tag{2}$$

Figure 4(a) shows that the inelastic signal at 50 meV is exceptional in that the strongest contribution originates from a graphene out-of-plane phonon mode. At the same time, an out-of-plane vibration of Pc contributes significantly to this signal. These observations lend evidence to the physical mechanism underlying the magnification of a graphene phonon via a single molecule, which requires the efficient coupling of lattice and molecule vibrations with matching symmetry. The mixing of vibrational quanta can be quantified by using the weights w_λ^X. Figure 4(b) shows the variation of $w_\lambda^{g_z} \cdot w_\lambda^{m_z}$ with the vibrational energy (the variation of other weights are presented in the Supplemental Material [40]). The product of weights is maximal if, for a particular mode λ, both graphene and Pc contribute equally. The latter applies to a vibrational mode at 50 meV, which for graphene represents an out-of-plane acoustic mode at the BZ M point [61,65], while it is a twisting vibration of all isoindole moieties of the molecule [58]. For several other modes, large products are attained, too; however, their inelastic scattering rate $\gamma_{\lambda,\sigma}$ is orders of magnitude lower [Fig. 4(a)]. These results demonstrate clearly that for the magnification of the graphene phonon mode, both ingredients are required, i.e., the adsorbate orbital resonance as well as the coupling between adsorbate and substrate vibrations.

The presented findings are unexpected. The current picture of enhanced inelastic electron transport relies on the presence of orbital resonances covering the relevant range of vibrational energies [19,22,66,67]. Importantly, in this picture, the resonance and vibrational excitations belong to one and the same quantum object. Examples are O_2 vibrations on Ag(110) [68–70], C_{60} Jahn-Teller modes on Pb(111) [21,23,24], as well as highly resolved molecular vibrational quanta on a superconductor [71]. In the present Letter, a resonance of an adsorbate, Pc, is used to enhance vibrations of the substrate, graphene. In this sense, the adsorbed molecule acts as a sensitive and local probe of graphene phonons. Moreover, the phonon-mediated tunneling mechanism [31] put forward as a rationale for the observed enhancement of phonon signals in IETS does not apply. Rather than the previously required match of electron and phonon momenta, the local breaking of symmetry due to the adsorbed molecule and the substrate surface is likely to provide final states for the inelastic tunneling electrons close to the BZ center.

In conclusion, an adsorbate orbital resonance magnifies spectroscopic signals of substrate phonons. To this end, besides the overlap of electronic and vibrational energies, the symmetry of atomic motions must match. In the presented case of 2H-Pc adsorbed on graphene-covered Ir(111), the molecular orbital resonance can be chemically engineered by pyrrolic-H abstraction, allowing a clear-cut correlation between the presence (absence) of the resonance and the appearance (nonappearance) of the magnified graphene phonon inelastic signal. The magnification is maximum at the center of the macrocyclic molecule, which turns the molecule into a local probe of the substrate vibrational quanta. Therefore, the findings open the path to locally explore phonon excitations at atom defects or impurities.

Funding by the Deutsche Forschungsgemeinschaft (Grant No. KR 2912/17-1) and Villum Fonden (Grant No. 00013340) is acknowledged. The Center for Nanostructured Graphene (CNG) is sponsored by the Danish Research Foundation (Grant No. DNRF103).

*joerg.kroeger@tu-ilmenau.de

[1] R. C. Jaklevic and J. Lambe, Phys. Rev. Lett. **17**, 1139 (1966).
[2] B. C. Stipe, M. A. Rezaei, and W. Ho, Science **280**, 1732 (1998).
[3] J. Lambe and S. L. McCarthy, Phys. Rev. Lett. **37**, 923 (1976).

[4] J. K. Gimzewski, J. K. Sass, R. R. Schlitter, and J. Schott, Europhys. Lett. **8**, 435 (1989).
[5] R. Berndt, J. K. Gimzewski, and P. Johansson, Phys. Rev. Lett. **67**, 3796 (1991).
[6] R. Berndt, R. Gaisch, J. K. Gimzewski, B. Reihl, R. R. Schlittler, W. D. Schneider, and M. Tschudy, Science **262**, 1425 (1993).
[7] X. H. Qiu, G. V. Nazin, and W. Ho, Science **299**, 542 (2003).
[8] A. J. Heinrich, J. A. Gupta, C. P. Lutz, and D. M. Eigler, Science **306**, 466 (2004).
[9] N. Lorente, R. Rurali, and H. Tang, J. Phys. Condens. Matter **17**, S1049 (2005).
[10] S.-W. Hla, J. Vac. Sci. Technol. B **23**, 1351 (2005).
[11] W. Ho, J. Chem. Phys. **117**, 11033 (2002).
[12] K. Morgenstern, N. Lorente, and K.-H. Rieder, Phys. Status Solidi (b) **250**, 1671 (2013).
[13] M. Galperin, M. A. Ratner, and A. Nitzan, J. Phys. Condens. Matter **19**, 103201 (2007).
[14] S. You, J.-T. Lü, J. Guo, and Y. Jiang, Adv. Phys. **2**, 907 (2017).
[15] N. Lorente and M. Persson, Phys. Rev. Lett. **85**, 2997 (2000).
[16] N. Lorente, M. Persson, L. J. Lauhon, and W. Ho, Phys. Rev. Lett. **86**, 2593 (2001).
[17] A. Gagliardi, G. C. Solomon, A. Pecchia, T. Frauenheim, A. Di Carlo, N. S. Hush, and J. R. Reimers, Phys. Rev. B **75**, 174306 (2007).
[18] M. Paulsson, T. Frederiksen, H. Ueba, N. Lorente, and M. Brandbyge, Phys. Rev. Lett. **100**, 226604 (2008).
[19] B. N. J. Persson and A. Baratoff, Phys. Rev. Lett. **59**, 339 (1987).
[20] M. Galperin, A. Nitzan, and M. A. Ratner, Phys. Rev. B **73**, 045314 (2006).
[21] K. J. Franke, G. Schulze, and J. I. Pascual, J. Phys. Chem. Lett. **1**, 500 (2010).
[22] K. J. Franke and J. I. Pascual, J. Phys. Condens. Matter **24**, 394002 (2012).
[23] S. Meierott, N. Néel, and J. Kröger, J. Phys. Chem. Lett. **7**, 2388 (2016).
[24] S. Meierott, N. Néel, and J. Kröger, Phys. Rev. B **96**, 205437 (2017).
[25] L. Vitali, M. A. Schneider, K. Kern, L. Wirtz, and A. Rubio, Phys. Rev. B **69**, 121414(R) (2004).
[26] J. Lee, K. Fujita, K. McElroy, J. A. Slezak, M. Wang, Y. Aiura, H. Bando, M. Ishikado, T. Masui, J.-X. Zhu, A. V. Balatsky, H. Eisaki, S. Uchida, and J. C. Davis, Nature (London) **442**, 546 (2006).
[27] H. Gawronski, M. Mehlhorn, and K. Morgenstern, Science **319**, 930 (2008).
[28] I. Altfeder, A. A. Voevodin, and A. K. Roy, Phys. Rev. Lett. **105**, 166101 (2010).
[29] K. Volgmann, H. Gawronski, C. Zaum, G. G. Rusina, S. D. Borisova, E. V. Chulkov, and K. Morgenstern, Nat. Commun. **5**, 5089 (2014).
[30] E. Minamitani, R. Arafune, N. Tsukahara, Y. Ohda, S. Watanabe, M. Kawai, H. Ueba, and N. Takagi, Phys. Rev. B **93**, 085411 (2016).
[31] Y. Zhang, V. W. Brar, F. Wang, C. Girit, Y. Yayon, M. Panlasigui, A. Zettl, and M. F. Crommie, Nat. Phys. **4**, 627 (2008).
[32] F. D. Natterer, Y. Zhao, J. Wyrick, Y.-H. Chan, W.-Y. Ruan, M.-Y. Chou, K. Watanabe, T. Taniguchi, N. B. Zhitenev, and J. A. Stroscio, Phys. Rev. Lett. **114**, 245502 (2015).
[33] T. O. Wehling, I. Grigorenko, A. I. Lichtenstein, and A. V. Balatsky, Phys. Rev. Lett. **101**, 216803 (2008).
[34] N. Néel, C. Steinke, T. O. Wehling, and J. Kröger, Phys. Rev. B **95**, 161410(R) (2017).
[35] J. Halle, N. Néel, M. Fonin, M. Brandbyge, and J. Kröger, Nano Lett. **18**, 5697 (2018).
[36] J. Kröger, N. Néel, T. O. Wehling, and M. Brandbyge, Small Methods **4**, 1900817 (2020).
[37] H. W. Kim, W. Ko, J. Ku, I. Jeon, D. Kim, H. Kwon, Y. Oh, S. Ryu, Y. Kuk, S. W. Hwang, and H. Suh, Nat. Commun. **6**, 7528 (2015).
[38] S.-Y. Li, K.-K. Bai, W.-J. Zuo, Y.-W. Liu, Z.-Q. Fu, W.-X. Wang, Y. Zhang, L.-J. Yin, J.-B. Qiao, and L. He, Phys. Rev. Appl. **9**, 054031 (2018).
[39] A. Allard and L. Wirtz, Nano Lett. **10**, 4335 (2010).
[40] See Supplemental Material at http://link.aps.org/supplemental/10.1103/PhysRevLett.130.116201, which includes Refs. [35,41–57], for experimental details on sample and tip preparation, enlarged views of spectroscopic data, the impact of shifted molecular resonances on inelastic signals, as well as data analysis tools and theoretical methods.
[41] N. Néel, M. Lattelais, M.-L. Bocquet, and J. Kröger, ACS Nano **10**, 2010 (2016).
[42] N. Papior, N. Lorente, T. Frederiksen, A. García, and M. Brandbyge, Comput. Phys. Commun. **212**, 8 (2017).
[43] J. P. Perdew, K. Burke, and M. Ernzerhof, Phys. Rev. Lett. **77**, 3865 (1996).
[44] T. Frederiksen, M. Paulsson, M. Brandbyge, and A.-P. Jauho, Phys. Rev. B **75**, 205413 (2007).
[45] J.-T. Lü, R. B. Christensen, G. Foti, T. Frederiksen, T. Gunst, and M. Brandbyge, Phys. Rev. B **89**, 081405(R) (2014).
[46] H. Hattab, A. T. N'Diaye, D. Wall, G. Jnawali, J. Coraux, C. Busse, R. van Gastel, B. Poelsema, T. Michely, F.-J. M. zu Heringdorf, and M. H. von Hoegen, Appl. Phys. Lett. **98**, 141903 (2011).
[47] L. Limot, J. Kröger, R. Berndt, A. Garcia-Lekue, and W. A. Hofer, Phys. Rev. Lett. **94**, 126102 (2005).
[48] J. Kröger, H. Jensen, and R. Berndt, New J. Phys. **9**, 153 (2007).
[49] J. Kröger, N. Néel, and L. Limot, J. Phys. Condens. Matter **20**, 223001 (2008).
[50] J. Kröger, N. Néel, A. Sperl, Y. F. Wang, and R. Berndt, New J. Phys. **11**, 125006 (2009).
[51] R. Berndt, J. Kröger, N. Néel, and G. Schull, Phys. Chem. Chem. Phys. **12**, 1022 (2010).
[52] I. Horcas, R. Fernández, J. M. Gómez-Rodríguez, J. Colchero, J. Gómez-Herrero, and A. M. Baro, Rev. Sci. Instrum. **78**, 013705 (2007).
[53] J. M. Soler, E. Artacho, J. D. Gale, A. García, J. Junquera, P. Ordejón, and D. Sánchez-Portal, J. Phys. Condens. Matter **14**, 2745 (2002).
[54] A. García *et al.*, J. Chem. Phys. **152**, 204108 (2020).
[55] M. Brandbyge, J.-L. Mozos, P. Ordejón, J. Taylor, and K. Stokbro, Phys. Rev. B **65**, 165401 (2002).
[56] N. Papior, G. Calogero, S. Leitherer, and M. Brandbyge, Phys. Rev. B **100**, 195417 (2019).

[57] N. Papior, P. Febrer, T. Frederiksen, N. Wittemeier, and A. Kole, sisl: v0.13.0 (2021), 10.5281/zenodo.7567793.
[58] M. Endlich, S. Gozdzik, N. Néel, A. L. da Rosa, T. Frauenheim, T. O. Wehling, and J. Kröger, J. Chem. Phys. **141**, 184308 (2014).
[59] N. Néel and J. Kröger, Molecules **22**, 731 (2017).
[60] S. J. Altenburg, J. Kröger, T. O. Wehling, B. Sachs, A. I. Lichtenstein, and R. Berndt, Phys. Rev. Lett. **108**, 206805 (2012).
[61] M. Endlich, A. Molina-Sánchez, L. Wirtz, and J. Kröger, Phys. Rev. B **88**, 205403 (2013).
[62] J. Tersoff and D. R. Hamann, Phys. Rev. Lett. **50**, 1998 (1983).
[63] J. Tersoff and D. R. Hamann, Phys. Rev. B **31**, 805 (1985).
[64] M. L. N. Palsgaard, N. P. Andersen, and M. Brandbyge, Phys. Rev. B **91**, 121403(R) (2015).
[65] M. Endlich, H. P. C. Miranda, A. Molina-Sánchez, L. Wirtz, and J. Kröger, Ann. Phys. (Berlin) **526**, 372 (2014).
[66] A. Baratoff and B. N. J. Persson, J. Vac. Sci. Technol. A **6**, 331 (1988).
[67] B. N. J. Persson, Phys. Scr. **38**, 282 (1988).
[68] J. R. Hahn, H. J. Lee, and W. Ho, Phys. Rev. Lett. **85**, 1914 (2000).
[69] M. Alducin, D. Sánchez-Portal, A. Arnau, and N. Lorente, Phys. Rev. Lett. **104**, 136101 (2010).
[70] S. Monturet, M. Alducin, and N. Lorente, Phys. Rev. B **82**, 085447 (2010).
[71] J. Homberg, A. Weismann, T. Markussen, and R. Berndt, Phys. Rev. Lett. **129**, 116801 (2022).